Supporting Information

Mechanistic Insights into Surface Chemical Interactions between Lithium Polysulfides and Transition Metal Oxides

Yiren Zhong, Ke R. Yang, Wen Liu, Peng He, Victor Batista, Hailiang Wang**

Department of Chemistry, Yale University, New Haven, Connecticut 06520, United States

Energy Sciences Institute, Yale University, West Haven, Connecticut 06516, United States

*E-mail: hailiang.wang@yale.edu (H.W.); victor.batista@yale.edu (V.S.B).

Synthesis of metal oxides:

The metal oxides of Mn, Fe, Co and Ni were synthesized with a general solvothermal method. Typically, 0.7 mmol of the corresponding metal acetate was dissolved in 35 mL of ethanol-water (10:1 v/v) mixed solution with continuous stirring for 10 min. The solution was then transferred to a 50 mL Teflon-lined stainless steel autoclave and heated at 160 ^{o}C for 12 h. After cooling to room temperature, the precipitate was collected by centrifuging and washing with water for three times. The final product was dried at 60 ^{o}C and ground for future use.

XPS study of interactions between LPS and oxides:

Metal oxide powder was uniformly dispersed in ethanol by sonication. The mixture was then drop-casted onto Al foil to form a film. The film was cut into a suitable size and immersed in a 0.01 M Li_2S_6 solution for 24 h to allow sufficient interaction with LPS. The Li_2S_6 solution was prepared by dissolving stoichiometric amounts of sulfur and lithium sulfide in a 1,3-dioxolane/dimethoxyethane (DOL/DME, 1:1 v/v) mixed solvent. After interaction, the metal oxide film was retrieved and transferred to the XPS chamber using a vacuum transfer vessel.

Material characterizations:

XRD was performed with a Rigaku SmartLab X-ray diffractometer with Cu Kα radiation (λ=1.5418 Å). SEM images were taken on a Hitachi SU8230 SEM microscope. XPS was performed on a PHI VersaProbe II Scanning XPS Microprobe with Al Kα monochromatic X-ray source.

Computational details:

We used the Vienna ab initio simulation package (VASP)[1-4] for all periodic boundary calculations. Projector augmented plane wave (PAW) method[5-6] together with the PBE exchange-correlation functional[7] were employed to describe the electron-ion interactions. We used the PBE + *U* method following Dudarev's approach[8] to add on-site potentials to the *d* electrons of transition metals to describe the electronic states of transition metal oxides properly. $U_{eff} = U - J$ parameters of 2 and 3 eV were used for Mn_3O_4 and Co_3O_4 to reproduce the experimental band gaps of bulk metal oxides. A cutoff of 450 eV was chosen for the plane wave basis set in all calculations. A 3 × 3 × 3 Monckhorst-Pack type k-point grid was chosen

for the optimization of bulk Mn_3O_4 and Co_3O_4. A Gaussian smear was used and the σ value was chosen to be 0.1 eV. The energy convergence criterion was set to be 10^{-4} eV per unit cell and the force convergence criterion of 0.01 eV $Å^{-1}$ was used for all structure optimization. As shown in Table S2 and S3, the calculated bulk properties of transition metal oxides agree well with experimental results.

Previous study[9] has shown that the (100) surface is the most stable surface of Co_3O_4 in terms of surface energy. More specifically, the (100) surface consisting of 4 five-coordinate Co(III) centers and 2 two-coordinate Co(II) centers is the most stable surface. For Mn_3O_4, previous computational study suggests that the (001) surface is the most stable surface.[10] Thus, we studied the absorption of Li_2S_x (x = 2-6) on Co_3O_4(100) and Mn_3O_4(001) surfaces. A vacuum slab of about 15 Å was inserted between the surface slab. The cell parameter is 23.12 Å × 8.12 Å × 8.12 Å for Co_3O_4(100) and 8.25 Å × 8.18 Å × 24.51 Å for Mn_3O_4(001). Standard Monkhorst-Pack k-point meshes of 1 × 3 × 3 and 3 × 3 × 1 were used for Co_3O_4(100) and Mn_3O_4(001), respectively. The bottom two metal-oxide layers of Co_3O_4 and Mn_3O_4 were fixed at the bulk position during geometry optimization. For the calculation of Li_2S_x, a supercell of 15 Å × 15 Å × 15 Å and a 1 × 1 × 1 Monkhorst-Pack k-point mesh were used. The binding energy (BE) was calculated as $BE = E_{total} - E_{ads} - E_{surf}$, where E_{total} is the total energy of the absorbed system, E_{ads} is the energy of the adsorbate (Li_2S_x) in vaccum and E_{surf} is the energy of the optimized bare surface.

We used Gaussian 09 software package[11] to calculate the change of the free energy of the two reactions shown in Figure S5 and S6. A pruned grid having 99 radial shells and 590 angular points per shell, called "ultrafine" grid in Gaussian 09, was used for the non-analytic integral evaluations. We used the PBE functional along with the Lanl2DZ pseudopotential and basis set[12] for Cu and 6-31G(d)[13-14] for other atoms in the geometry optimization and frequency analysis. The calculated vibrational frequencies were used for the computation of molecular partition functions to evaluate thermal contributions to the free energy at 298.15 K by employing the ideal gas, rigid rotator, harmonic oscillator approximation.[15] Single point calculations were performed at the optimized structures with the Lanl2DZ pseudopotential and basis set for Cu and the 6-311+G(2df,p) basis set[14] for other atoms for more reliable energetics. Since the direct calculation of the free energy of solids is not that straight forward, experimental formation free energies (Table S4) of CuO(s), Cu_2O(s), Li_2O(s), and Cu(g), and Li(g) were used to calculate the free energy changes of proposed reactions 1 and 2 according to the thermodynamic cycles in Figure S5 and S6. The structures of Li_2S_6, Li_2S_8, $Li_2S_2O_3$, and $Li_3[Cu(S_2O_3)_2]$ are shown in Figure S7 and their calculated solvation free energies are shown in Table S5. The solvation free energies were estimated with SMD solvation model[16] with diethyl ether as the solvent, since the parameters of DME and DOL are not implemented in Gaussian.

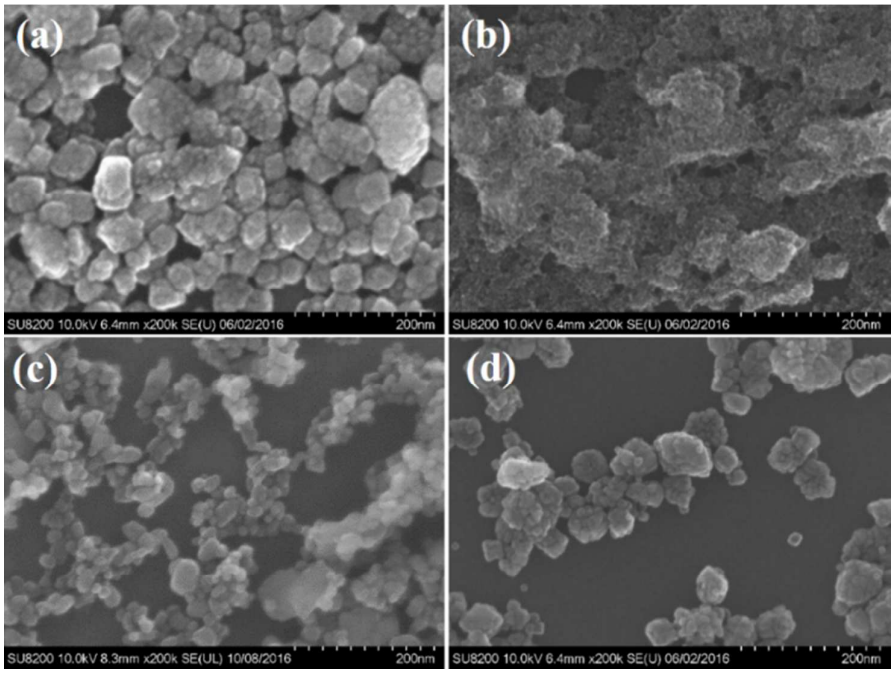

Figure S1. SEM images of (a) Co_3O_4, (b) Fe_2O_3, (c) Mn_3O_4 and (d) CuO.

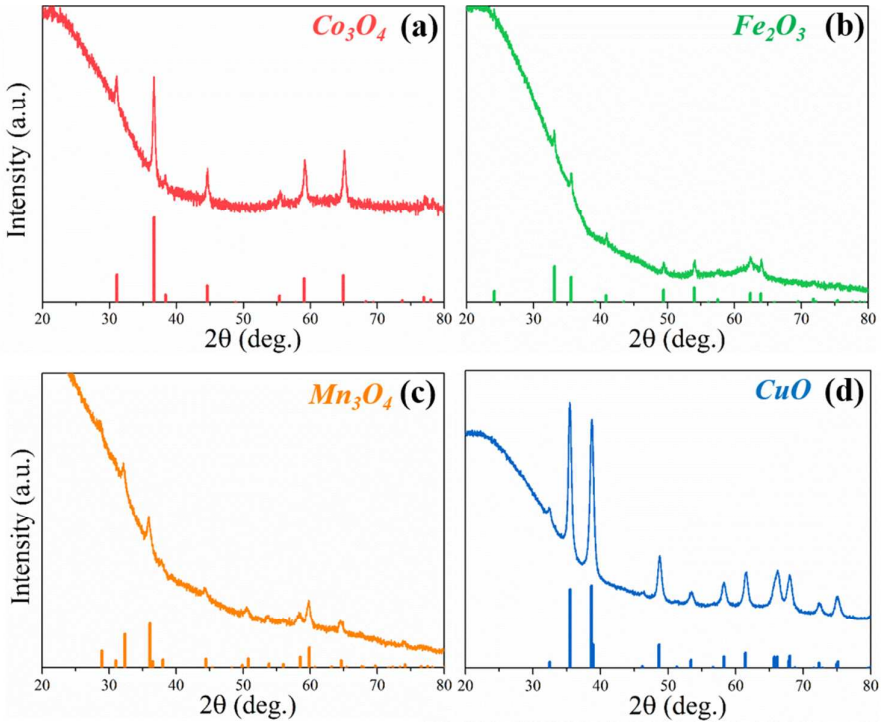

Figure S2. XRD of (a) Co_3O_4, (b) Fe_2O_3, (c) Mn_3O_4 and (d) CuO.

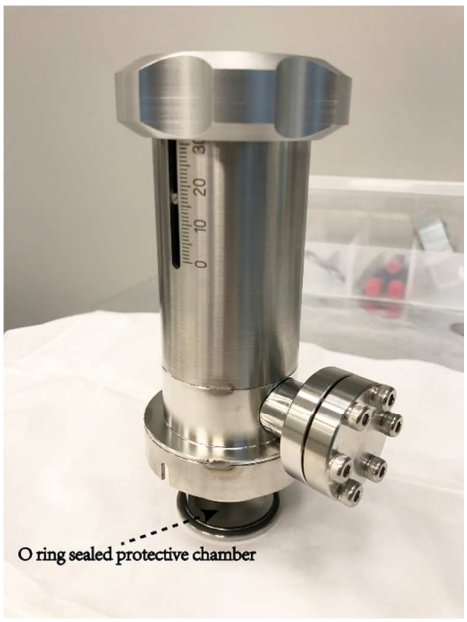

Figure S3. Picture of the vacuum vessel for XPS sample transfer.

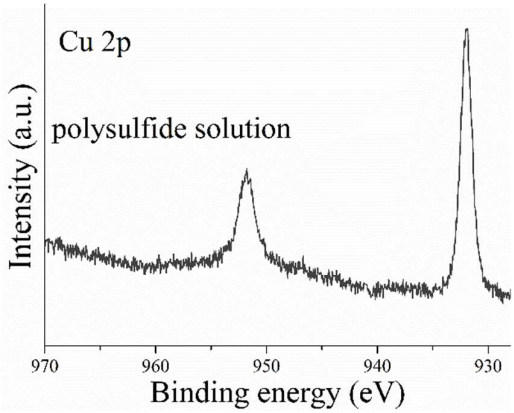

Figure S4. Cu 2p XPS spectra of the dried LPS solution after interacting with CuO.

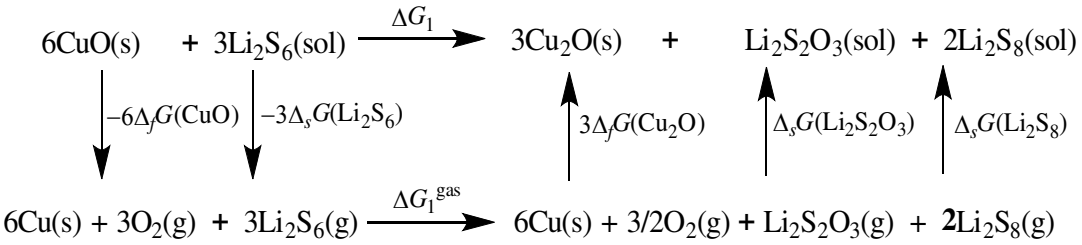

Figure S5. The thermodynamic cycle used to calculate the change of free energy for reaction 1.

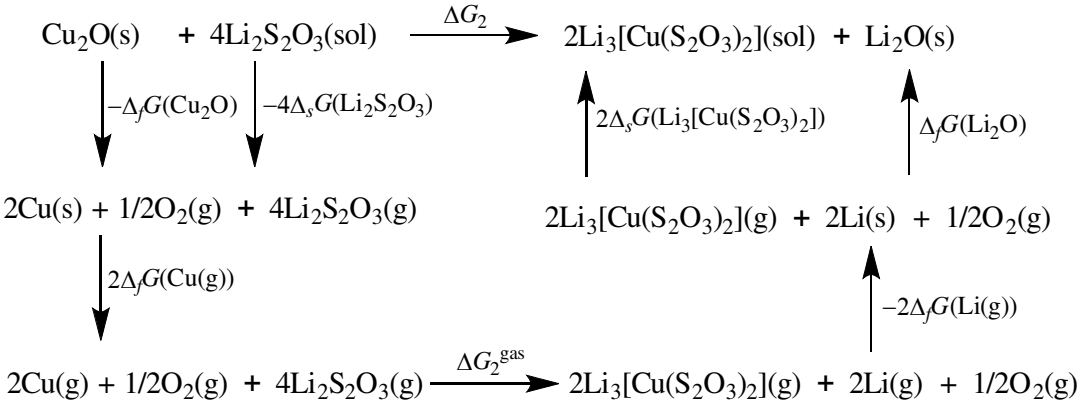

Figure S6. The thermodynamic cycle used to calculate the change of free energy for reaction 2.

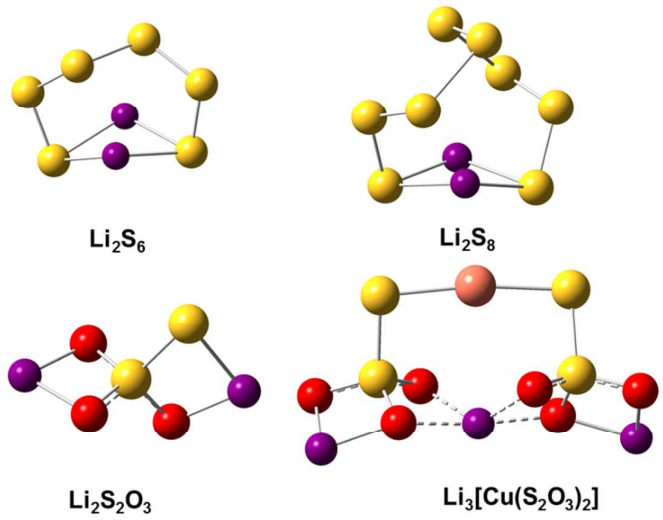

Figure S7. DFT optimized structures of Li_2S_6, Li_2S_8, $Li_2S_2O_3$, and $Li_3[Cu(S_2O_3)_2]$.

Table S1. Solubility product constants of sulfides of Mn, Fe, Co and Cu.

Solubility Product Constant (K_{sp}, 25 °C)			
MnS	FeS	CoS	CuS
3×10^{-11}	8×10^{-19}	3×10^{-26}	8×10^{-37}

Table S2. Calculated and experimental properties of bulk Mn_3O_4

Properties	PBE	PBE + U [a]	Expt.
a /Å	5.75	5.80	5.76[b]
b /Å	5.76	5.80	5.76[b]
c /Å	9.49	9.52	9.46[b]
dMn^{II}–O (Å)	2.00	2.03	2.07[b]
dMn^{III}–Oaxial (Å)	2.33	2.32	2.29[b]
dMn^{III}–Oequatorial (Å)	1.93	1.95	1.91[b]
Mn^{II} magnetic moment (μB)	4.18	4.42	4.34[c]
Mn^{III} magnetic moment (μB)	3.51	3.73	3.45[c]
Eg (eV)	0.96	1.30	1.91[d]

[a] A $U - J$ value of 2.0 eV was used in the calculation.
[b] Ref. [17].
[c] Ref. [18].
[d] Ref. [19].

Table S3. Calculated and experimental properties of bulk Co_3O_4

Properties	PBE	PBE + U[a]	Expt.
unit cell parameter/Å	8.09	8.12	8.082[b]
dCo^{II}–O (Å)	1.92	1.95	1.928[b]
dCo^{III}–O (Å)	1.93	1.92	1.923[b]
Atomic magnetic moment (μB)	2.25	2.61	3.26[c]
E_g (eV)	0.18	1.48	1.60[d]

[a] A $U - J$ value of 3.0 eV was used in the calculation.
[b] Ref. [20].
[c] Ref. [21].
[d] Ref. [22].

Table S4. Experimental standard molar Gibbs energies of formation for metal oxides and metal atoms at 298.15 K[a]

	kJ mol^{-1}	kcal mol^{-1}
CuO(s)	-129.7	-31.0
Cu_2O(s)	-146.0	-34.9
Li_2O(s)	-561.2	-134.1
Li(g)	126.6	30.3
Cu(g)	297.7	71.2

[a] Experimental data taken from [23].

Table S5. Calculated Gibbs free energies of solvation

	kcal mol^{-1}
Li_2S_6	-12.7
Li_2S_8	-12.5
$Li_2S_2O_3$	-18.9
$Li_3[Cu(S_2O_3)_2]$	-28.7

REFERENCES

1. Kresse, G.; Hafner, J. Ab Initio Molecular Dynamics for Liquid Metals. *Phys. Rev. B* **1993,** *47*, 558-561.

2. Kresse, G.; Hafner, J. Ab Initio Molecular-Dynamics Simulation of the Liquid-Metal–Amorphous-Semiconductor Transition in Germanium. *Phys. Rev. B* **1994,** *49*, 14251-14269.

3. Kresse, G.; Furthmüller, J. Efficiency of Ab-Initio Total Energy Calculations for Metals and Semiconductors Using a Plane-Wave Basis Set. *Comput. Mater. Sci.* **1996,** *6*, 15-50.

4. Kresse, G.; Furthmüller, J. Efficient Iterative Schemes for Ab Initio Total-Energy Calculations Using a Plane-Wave Basis Set. *Phys. Rev. B* **1996,** *54*, 11169-11186.

5. Blöchl, P. E. Projector Augmented-Wave Method. *Phys. Rev. B* **1994,** *50*, 17953-17979.

6. Kresse, G.; Joubert, D. From Ultrasoft Pseudopotentials to the Projector Augmented-Wave Method. *Phys. Rev. B* **1999,** *59*, 1758-1775.

7. Perdew, J. P.; Burke, K.; Ernzerhof, M. Generalized Gradient Approximation Made Simple. *Phys. Rev. Lett.* **1996,** *77*, 3865-3868.

8. Dudarev, S. L.; Botton, G. A.; Savrasov, S. Y.; Humphreys, C. J.; Sutton, A. P. Electron-Energy-Loss Spectra and the Structural Stability of Nickel Oxide: An LSDA+U Study. *Phys. Rev. B* **1998,** *57*, 1505-1509.

9. Zasada, F.; Piskorz, W.; Stelmachowski, P.; Kotarba, A.; Paul, J.-F.; Płociński, T.; Kurzydłowski, K. J.; Sojka, Z. Periodic DFT and HR-STEM Studies of Surface Structure and Morphology of Cobalt Spinel Nanocrystals. Retrieving 3D Shapes from 2D Images. *J. Phys. Chem. C* **2011,** *115*, 6423-6432.

10. Bayer, V.; Podloucky, R.; Franchini, C.; Allegretti, F.; Xu, B.; Parteder, G.; Ramsey, M. G.; Surnev, S.; Netzer, F. P. Formation of Mn_3O_4 (001) on MnO (001): Surface and Interface Structural Stability. *Phys. Rev. B* **2007,** *76*, 165428-165438.

11. Frisch, M. J.; Trucks, G. W.; Schlegel, H. B.; Scuseria, G. E.; Robb, M. A.; Cheeseman, J. R.; Scalmani, G. B., V. ; Mennucci, B.; Petersson, G. A., et al. *Gaussian 09*, Rev. D.01; Gaussian, Inc.: Wallingford, CT, 2009.

12. Hay, P. J.; Wadt, W. R. Ab Initio Effective Core Potentials for Molecular Calculations. Potentials for K to Au Including the Outermost Core Orbitals. *J. Chem. Phys.* **1985,** *82*, 299-310.

13. Francl, M. M.; Pietro, W. J.; Hehre, W. J.; Binkley, J. S.; Gordon, M. S.; DeFrees, D. J.; Pople, J. A. Self□Consistent Molecular Orbital Methods. XXIII. A Polarization□Type Basis Set for Second□Row Elements. *J. Chem. Phys.* **1982,** *77*, 3654-3665.

14. Frisch, M. J.; Pople, J. A.; Binkley, J. S. Self□Consistent Molecular Orbital Methods 25. Supplementary Functions for Gaussian Basis Sets. *J. Chem. Phys.* **1984,** *80*, 3265-3269.

15. Cramer, C. J. *Essentials of Computational Chemistry: Theories and Models. 2nd ed.*; Wiley: Chichester, U. K., 2004.

16. Marenich, A. V.; Cramer, C. J.; Truhlar, D. G. Universal Solvation Model Based on Solute Electron Density and on a Continuum Model of the Solvent Defined by the Bulk Dielectric Constant and Atomic Surface Tensions. *J. Phys. Chem. B* **2009,** *113*, 6378-6396.

17. Satomi, K. Oxygen Positional Parameters of Tetragonal Mn_3O_4. *J. Phys. Soc. Jpn.* **1961,** *16*, 258-266.

18. Jensen, G. B.; Nielsen, O. V. The Magnetic Structure of Mn_3O_4 Hausmannite between 4.7K and Neel Point, 41K. *J. Phys. C: Solid State Phys.* **1974,** *7*, 409-424.

19. Lim, J. S.; Saldana-Greco, D.; Rappe, A. M. Improved Pseudopotential Transferability for Magnetic and Electronic Properties of Binary Manganese Oxides from DFT+U+J Calculations. *Phys.*

Rev. B **2016,** *94*, 165151-165161.

20. Liu, X.; Prewitt, C. T. High-Temperature X-Ray Diffraction Study of Co_3O_4: Transition from Normal to Disordered Spinel. *Phys. Chem. Mineral.* **1990,** *17*, 168-172.

21. Roth, W. L. The Magnetic Structure of Co_3O_4. *J. Phys. Chem. Solids* **1964,** *25*, 1-10.

22. Shinde, V. R.; Mahadik, S. B.; Gujar, T. P.; Lokhande, C. D. Supercapacitive Cobalt Oxide (Co_3O_4) Thin Films by Spray Pyrolysis. *Appl. Surf. Sci.* **2006,** *252*, 7487-7492.

23. Haynes, W. M. *Standard Thermodynamics Properties of Chemical Substances*. *97th Edition (Internet Version 2017) ed.*; CRC Press/Taylor & Francis: Boca Raton, FL, 2017.